DISEASES AND DISORDERS

β-arrestin-1 suppresses myogenic reprogramming of brown fat to maintain euglycemia

Sai P. Pydi[1]*, Shanu Jain[1], Luiz F. Barella[1], Lu Zhu[1], Wataru Sakamoto[1], Jaroslawna Meister[1], Lei Wang[1], Huiyan Lu[2], Yinghong Cui[1], Oksana Gavrilova[3], Jürgen Wess[1]*

Copyright © 2020 The Authors, some rights reserved; exclusive licensee American Association for the Advancement of Science. No claim to original U.S. Government Works. Distributed under a Creative Commons Attribution NonCommercial License 4.0 (CC BY-NC).

A better understanding of the signaling pathways regulating adipocyte function is required for the development of new classes of antidiabetic/obesity drugs. We here report that mice lacking β-arrestin-1 (barr1), a cytoplasmic and nuclear signaling protein, selectively in adipocytes showed greatly impaired glucose tolerance and insulin sensitivity when consuming an obesogenic diet. In contrast, transgenic mice overexpressing barr1 in adipocytes were protected against the metabolic deficits caused by a high-calorie diet. Barr1 deficiency led to a myogenic reprogramming of brown adipose tissue (BAT), causing elevated plasma myostatin (Mstn) levels, which in turn led to impaired insulin signaling in multiple peripheral tissues. Additional in vivo studies indicated that barr1-mediated suppression of Mstn expression by BAT is required for maintaining euglycemia. These findings convincingly identify barr1 as a critical regulator of BAT function. Strategies aimed at enhancing barr1 activity in BAT may prove beneficial for the treatment of type 2 diabetes.

INTRODUCTION

Type 2 diabetes (T2D) represents a major metabolic disease that has emerged as a serious health problem worldwide (*1*). The key factor responsible for the ever-increasing number of patients with T2D is the global obesity epidemic (*2*–*4*).

Adipocytes play a key role in the pathogenesis of T2D (*5*). When energy intake exceeds energy expenditure, adipocytes undergo hypertrophy and macrophage infiltration, resulting in the secretion of inflammatory adipokines and other factors that promote peripheral insulin resistance and impaired glucose homeostasis (*3*, *4*, *6*, *7*). Both white and brown adipose tissues (WAT and BAT, respectively) secrete many shared adipokines, but BAT also releases adipokines that are unique to thermogenic cells (*8*, *9*). Clearly, a better understanding of the signaling pathways that regulate adipocyte function under physiological and pathophysiological conditions is essential for developing new pharmacological strategies to combat the ongoing obesity/T2D epidemic.

During the past few years, we used mouse genetics to identify pathways and signaling proteins that regulate adipocyte function and whole-body glucose homeostasis (*10*, *11*). In the present study, we generated and analyzed a mouse strain that selectively lacked β-arrestin-1 (barr1) in adipocytes [adipo-barr1-KO (knockout) mice]. Barr1 and barr2 are intracellular proteins that are well known for their ability to terminate signaling through G protein (heterotrimeric GTP-binding protein)–coupled receptors (GPCRs) (*12*, *13*). However, barr1/2 can also act as signaling proteins in their own right (*14*–*16*). Although barr1 and barr2 show a high degree of sequence homology, they can have divergent functions in various cell types (*17*). In agreement with this finding, barr1, but not barr2, can interact with nuclear transcription factors ((*18*, *19*).

We made the unexpected observation that adipo-barr1-KO mice displayed metabolic phenotypes that were opposite to those observed with adipo-barr2-KO mice (*10*). Using loss- and gain-of-function mouse models, we demonstrated that barr1 suppresses myogenic reprogramming of BAT to maintain euglycemia and that altered myostatin (Mstn) expression by BAT plays a key role in mediating the observed metabolic phenotypes. We also delineated a molecular pathway through which barr1 exerts its inhibitory effect on Mstn expression in BAT. Our findings strongly suggest that strategies aimed at enhancing barr1 expression or activity in BAT may prove beneficial for the treatment of T2D.

RESULTS

Generation of adipo-barr1-KO mice

To investigate the potential physiological roles of barr1 expressed by adipose tissue, we inactivated the *barr1* gene selectively in mouse adipocytes. Specifically, we crossed floxed *barr1* mice (*barr1 f/f* mice; genetic background: C57BL/6J) (*20*) with mice expressing Cre recombinase under the control of the adipocyte-specific adiponectin promoter (*adipoq-Cre* mice) (*21*). These matings yielded floxed *barr1* mice carrying the *adipoq-Cre* transgene (*adipoq-Cre-barr1 f/f* mice) and *barr1 f/f* control littermates. Quantitative reverse transcription polymerase chain reaction (qRT-PCR) studies showed that *barr1* mRNA levels were selectively reduced in adipose tissues [subcutaneous inguinal fat (iWAT), epididymal fat (eWAT), and BAT] of *adipoq-Cre-barr1 f/f* mice (Fig. 1A). In agreement with the RNA expression data, Western blot studies confirmed that barr1 protein levels were markedly decreased in mature adipocytes prepared from iWAT, eWAT, and BAT of *adipoq-Cre barr1 f/f* mice (Fig. 1B). The expression levels of *barr1* in other metabolically important tissues were similar in *adipoq-Cre barr1 f/f* and control mice (Fig. 1A). Additional qRT-PCR studies showed that adipocyte *barr1* deficiency did not cause any compensatory changes in the expression levels of *barr2* (fig. S1A).

[1]Molecular Signaling Section, Laboratory of Bioorganic Chemistry, National Institute of Diabetes and Digestive and Kidney Diseases, Bethesda, MD 20892, USA. [2]Mouse Transgenic Core Facility, National Institute of Diabetes and Digestive and Kidney Diseases, Bethesda, MD 20892, USA. [3]Mouse Metabolism Core, National Institute of Diabetes and Digestive and Kidney Diseases, Bethesda, MD 20892, USA.
*Corresponding author. Email: jurgenw@niddk.nih.gov (J.W.); saiprasad.pydi@nih.gov (S.P.P.)

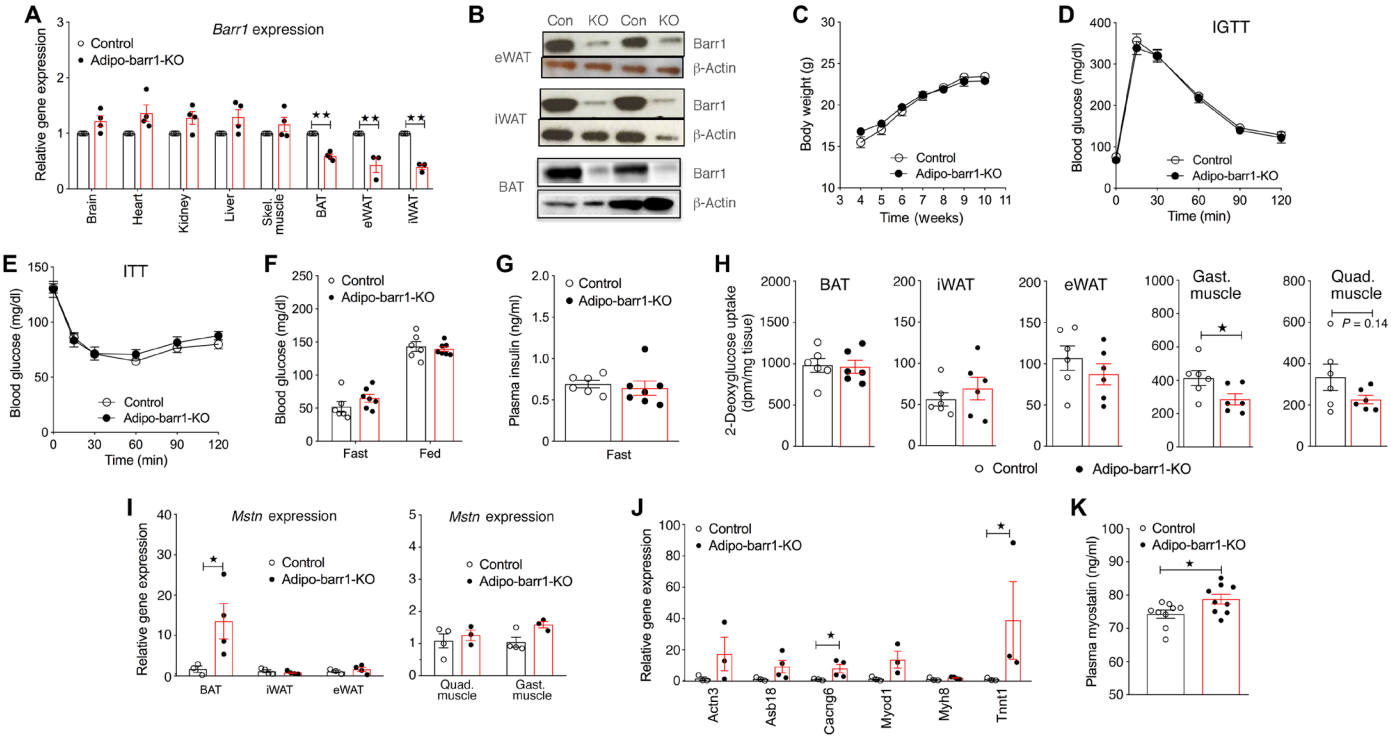

Fig. 1. Lack of barr1 in adipocytes decreases glucose uptake by skeletal muscle and increases the expression of myogenic genes in BAT. All studies were performed with male mice consuming regular chow (RC) mouse. (**A**) Expression of *barr1* mRNA in different tissues of *adipoq-Cre barr1 f/f* mice and control littermates (*barr1 f/f*). *Barr1* expression was normalized relative to the expression of 18*S* ribosomal RNA ($n = 3$). Throughout the manuscript, the *adipoq-Cre barr1 f/f* mice are referred to as adipo-barr1-KO mice. (**B**) Protein expression levels of barr1 in mature adipocytes from iWAT, eWAT, and BAT. (**C**) Body weight measurements ($n = 6$ or 7). (**D**) Intraperitoneal glucose tolerance test (IGTT; 2 g of glucose per kilogram, ip) ($n = 6$ or 7). (**E**) Insulin tolerance test (ITT; 0.75 U/kg, ip) ($n = 6$ or 7). (**F**) Fasting and fed blood glucose levels ($n = 6$ or 7). (**G**) Fasting plasma insulin levels ($n = 6$ or 7). (**H**) In vivo 2-deoxyglucose uptake studies. Adipo-barr1-KO mice and control littermates received an intraperitoneal insulin injection (0.75 U/kg). Insulin-stimulated glucose uptake into iWAT, eWAT, BAT, and quadriceps and gastrocnemius muscles was studied using the 2-deoxyglucose method ($n = 6$). (**I**) mRNA expression levels of *Mstn* in BAT, iWAT, eWAT, and quadriceps and gastrocnemius muscles in adipo-barr1-KO and control mice ($n = 3$ or 4). (**J**) Expression of myogenic genes in BAT of adipo-barr1-KO and control mice ($n = 3$ or 4). (**K**) Plasma Mstn levels ($n = 8$ or 9). All data are expressed as means ± SEM. $^{\star}P < 0.05$ and $^{\star\star}P < 0.01$ (two-tailed Student's *t* test).

Throughout the text, we refer to the *adipoq-Cre barr1 f/f* mice simply as "adipo-barr1-KO mice."

Adipo-barr1-KO mice show decreased glucose uptake by skeletal muscle and increased myogenic gene expression in BAT

We initially subjected adipo-barr1-KO mice and their control littermates consuming a regular chow (RC) diet to a series of metabolic tests. The two groups of mice showed similar body weight, glucose tolerance, insulin sensitivity, and fed and fasting blood glucose and plasma insulin levels (Fig. 1, C to G). Moreover, plasma glycerol and triglyceride levels did not differ significantly between the two cohorts of mice (fig. S1, B and C). We next studied the effect of exogenously administered insulin on glucose uptake by metabolically important tissues. After a 16-hour fast, we injected adipo-barr1-KO mice and their control littermates with insulin [Humulin (0.75 U/kg), intraperitoneally (ip)] and a trace amount of 2-deoxy-D-[1-^{14}C] glucose. Forty minutes later, mice were euthanized, and tissues were collected for the measurement of glucose uptake (2-deoxy-D-[1-^{14}C] glucose-6P accumulation). During the test, none of the mice showed severe hypoglycemia (average blood glucose levels remained above 60 mg/dl). Glucose uptake by BAT, iWAT, and eWAT did not differ significantly between the two groups of mice (Fig. 1H). Glucose uptake was markedly decreased in gastrocnemius muscle, and a similar trend was observed with quadriceps muscle (Fig. 1H). Glucose uptake by other metabolically relevant tissues, including the brain, liver, and heart, did not differ significantly between adipo-barr1-KO and control mice (fig. S1D).

We hypothesized that the decrease in glucose uptake by skeletal muscle caused by the lack of barr1 in adipocytes might be due to altered secretion of adipokines or batokines (secreted factors preferentially released by BAT) from fat tissue. Two recent studies reported that BAT can secrete Mstn, an effect that could be linked to reduced insulin sensitivity and impaired exercise capacity, respectively (*22*, *23*). We therefore examined *Mstn* expression in different adipose tissue depots of adipo-barr1-KO mice and control littermates. We found that *Mstn* expression was increased 15-fold in BAT of adipo-barr1-KO mice, but not in iWAT and eWAT lacking barr1 (Fig. 1I). In addition to *Mstn*, the expression of several other myogenic genes was markedly increased in BAT of adipo-barr1-KO mice (Fig. 1J), but not in iWAT and eWAT (fig. S1, E and F). *Mstn* expression by skeletal muscle tissues was not significantly affected by the barr1 mutation (Fig. 1I). The enhanced expression of *Mstn* in BAT of the barr1 mutant mice was associated with a significant increase in plasma Mstn levels (Fig. 1K), raising the possibility that elevated plasma Mstn levels contribute to

the reduced glucose uptake by skeletal muscle caused by adipocyte barr1 deficiency.

Adipo-barr1-KO mice show pronounced metabolic impairments on an obesogenic diet

We also challenged adipo-barr1-KO mice and their control littermates with a high-fat diet (HFD) to induce obesity and obesity-associated metabolic deficits including glucose intolerance and insulin resistance. Both groups of mice were maintained on the obesogenic HFD for at least 8 weeks. Adipo-barr1-KO mice gained slightly more weight than their control littermates (Fig. 2A). However, body composition (% fat versus % lean mass) was similar in both groups of mice (Fig. 2B).

HFD adipo-barr1-KO mice showed pronounced impairments in glucose tolerance and insulin sensitivity, as compared to their HFD control littermates (Fig. 2, C and D). In contrast, glucose-stimulated insulin secretion (GSIS) was not significantly different between the two groups of mice (Fig. 2E). HFD barr1 mutant mice displayed markedly higher blood glucose and plasma insulin levels under both fasting and fed conditions (Fig. 2, F and G), consistent with peripheral insulin resistance. Plasma free fatty acid (FFA) and leptin levels (fed conditions) were also slightly increased in the HFD adipo-barr1-KO mice (Fig. 2, H and I).

While plasma adiponectin levels were decreased in the HFD adipo-barr1-KO mice (fasting conditions; Fig. 2J), the plasma levels of monocyte chemoattractant protein 1 (MCP1) and tumor necrosis factor–α (TNFα), two proinflammatory cytokines, were significantly elevated in the HFD barr1 mutant mice (Fig. 2, K and L). Similar to the RC barr1 mutant mice, the HFD adipo-barr1-KO mice also showed a marked increase in the plasma levels of Mstn (Fig. 2M).

To examine whether the lack of barr1 in adipocytes affected whole-body energy homeostasis, we performed a series of indirect calorimetry measurements (fig. S2). HFD adipo-barr1-KO and control mice showed no significant differences in total energy expenditure (TEE), food intake, oxygen consumption rate, and locomotor activity (fig. S2, A to D).

Hyperinsulinemic-euglycemic clamp study confirms that adipo-barr1-KO HFD mice are insulin resistant

To study insulin sensitivity and glucose fluxes in HFD adipo-barr1-KO and control mice in more detail, we performed a hyperinsulinemic-euglycemic clamp study (Fig. 3, A to F). Mice received insulin at a rate of 3 mU/min per kilogram, and euglycemia was maintained by infusing variable amounts of glucose (Fig. 3A). The glucose infusion rate (GIR) was markedly reduced in HFD adipo-barr1-KO mice as compared with control littermates (Fig. 3, B and C), indicating

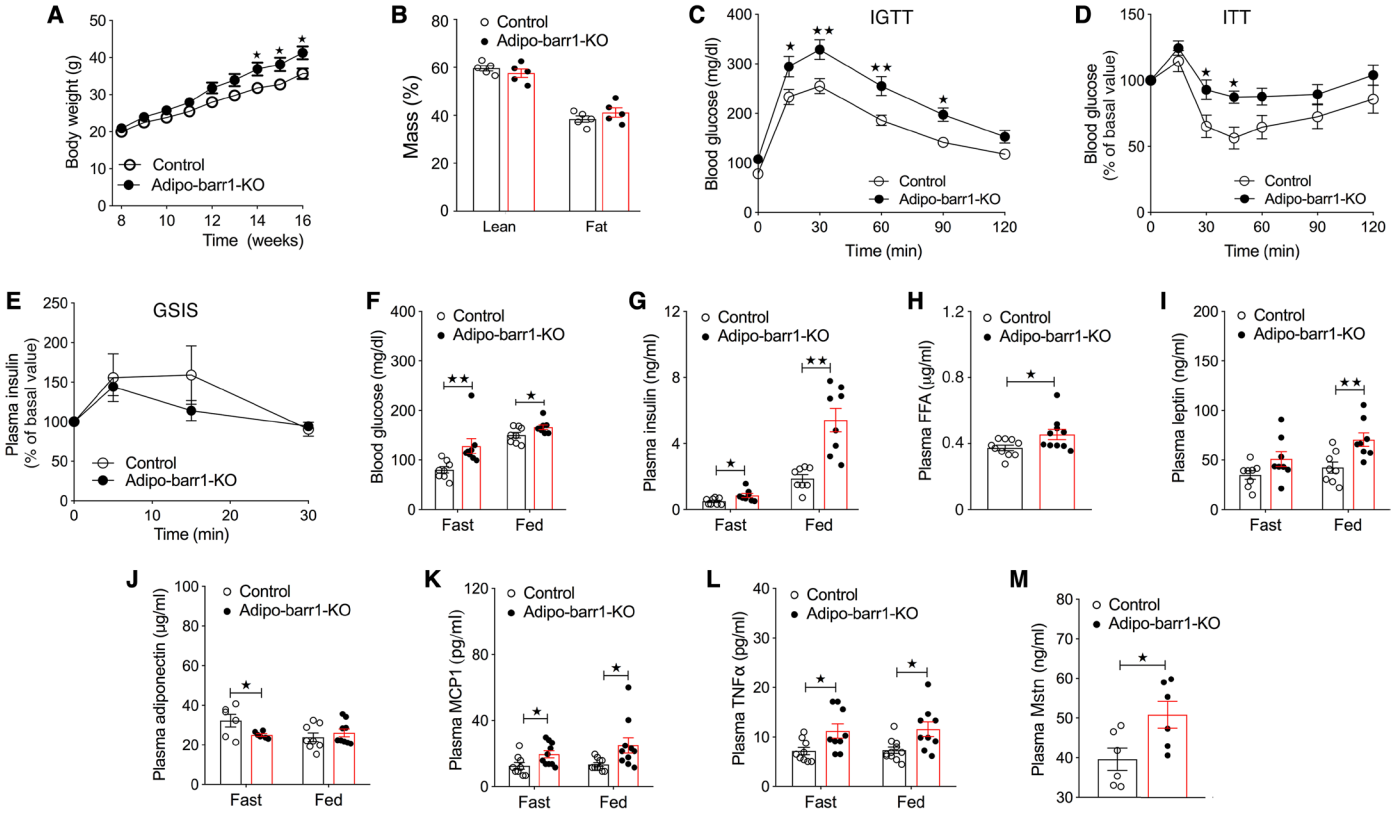

Fig. 2. An obesogenic diet causes severe metabolic deficits in adipo-barr1-KO mice. All studies were carried out with male mice consuming a HFD for at least 8 weeks. (**A**) Body weights of control and adipo-barr1-KO mice consuming a HFD ($n = 5$ to 7). (**B**) Body composition in percentage (fat versus lean mass) of mice maintained on an HFD for 12 weeks ($n = 5$). (**C**) IGTT (1 g of glucose per kilogram, ip). (**D**) ITT (0.75 U/kg, ip). (**E**) GSIS (2 g of glucose per kilogram, ip). (**F** and **G**) Fasting and fed blood glucose (F) and plasma insulin (G) levels. (**H**) Fasting plasma free fatty acid (FFA) levels. (**I** to **L**) Plasma leptin (I), adiponectin (J), MCP1 (K), and tumor necrosis factor–α (L) levels in fasting and fed HFD adipo-barr1-KO and control mice. (**M**) Plasma Mstn levels in HFD adipo-barr1-KO and control mice ($n = 6$). Data represent means ± SEM (C to L, $n = 6$ to 10). $^*P < 0.05$ and $^{**}P < 0.01$ [(B and F) to two-tailed Student's t test; (A), (C), and (D) two-way analysis of variance (ANOVA) followed by Bonferroni's post hoc test].

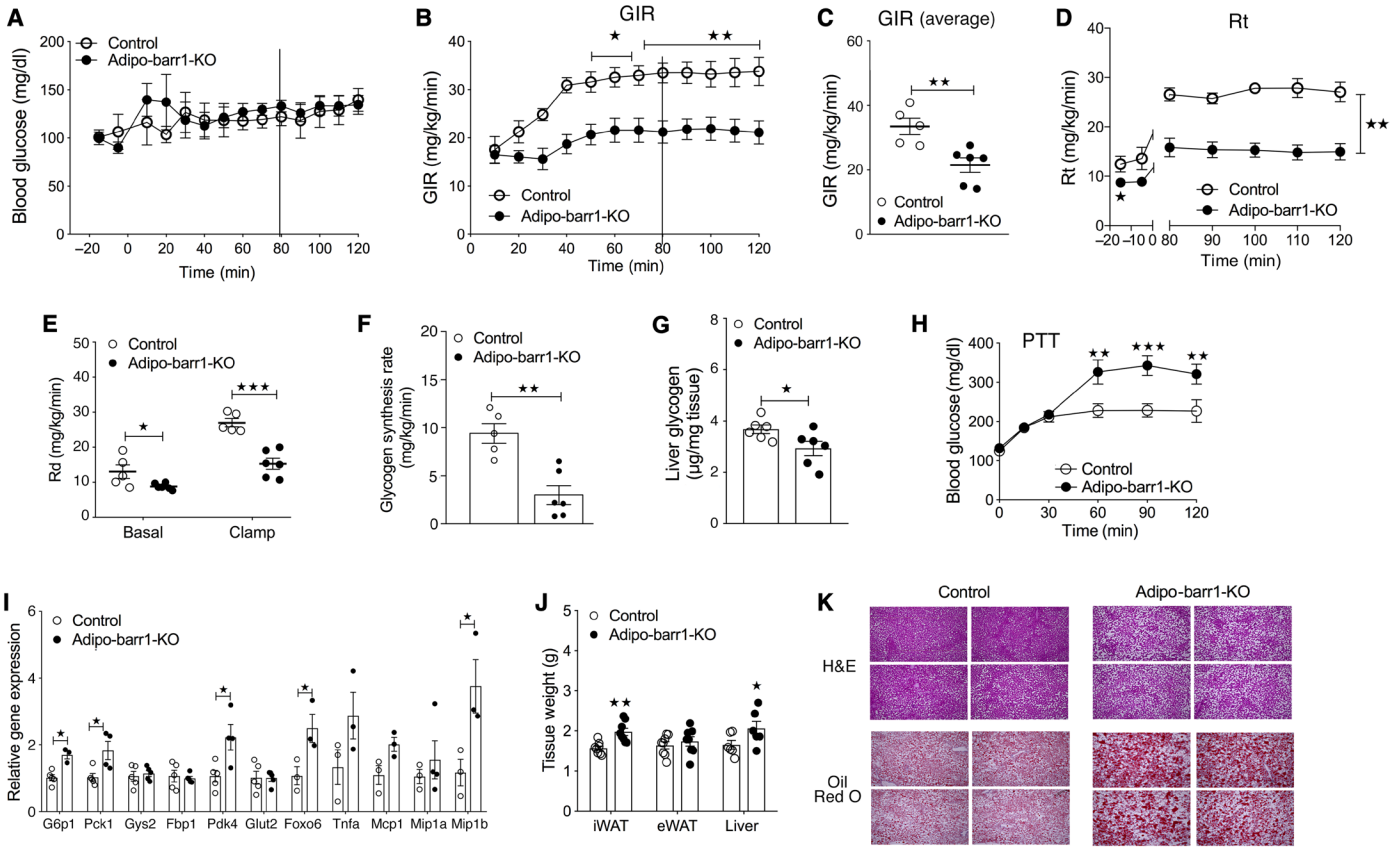

Fig. 3. Hyperinsulinemic-euglycemic clamp study confirms that HFD adipo-barr1-KO HFD mice are insulin resistant. Experiments were carried out with adipo-barr1-KO and control mice (males) that had been maintained on an HFD for 12 weeks. (**A**) Blood glucose levels during the clamp study ($n = 5$ or 6). (**B** and **C**) GIR ($n = 5$ or 6). (**D**) Glucose turnover rate (Rt) ($n = 5$ or 6). (**E** and **F**) Rates of glucose disappearance (Rd) (E) and glycogen synthesis (F) ($n = 4$ to 6). (**G**) Liver glycogen levels of HFD adipo-barr1-KO and control mice ($n = 5$ or 6). (**H**) Pyruvate tolerance test (PTT, 2 g of pyruvate per kilogram, ip) carried out with HFD adipo-barr1-KO and control mice ($n = 5$ or 6). (**I**) Expression levels of genes involved in glucose metabolism and inflammatory responses (proinflammatory cytokines) in HFD adipo-barr1-KO and control mice ($n = 3$ to 5). (**J**) Tissue weights of adipo-barr1-KO and control mice maintained on HFD for 12 weeks ($n = 5$ or 6). (**K**) Hematoxylin and eosin (H&E) and Oil O Red staining of liver sections from HFD adipo-barr1-KO and control mice ($n = 3$). Data represent means ± SEM. $^{\star}P < 0.05$, $^{\star\star}P < 0.01$, and $^{\star\star\star}P < 0.001$. [(C to G), (I), and (J) two-tailed Student's *t* test; (B and H) two-way ANOVA followed by Bonferroni's post hoc test].

that the mutant mice were insulin resistant. During the clamp, the glucose turnover rate (Rt; Fig. 3D) and the rate of glucose disappearance (Rd; Fig. 3E) were significantly decreased in the HFD barr1 mutant mice. The mutant mice also displayed a marked reduction in glycogen synthesis rate (Fig. 3F). Hepatic glucose production (HGP) and glycolysis rate did not differ significantly between the two groups of mice (fig. S3, A and B). Together, these findings clearly indicate that lack of barr1 in adipocytes results in severe systemic insulin resistance. Consistent with the data shown in Fig. 2A, the HFD adipo-barr1-KO mutant mice used for the clamp studies weighed ~10% more than their control littermates (KO, 50.1 ± 1.7 g; control, 45.6 ± 2.4 g; $P < 0.05$, $n = 5$ or 6 per group).

Lack of barr1 in adipocytes causes impaired liver glucose metabolism

Since the clamp data indicated that glycogen synthesis rate was reduced in the HFD adipo-barr1-KO mice (Fig. 3F), we measured hepatic glycogen content in HFD barr1 mutant mice and control littermates. We found that hepatic glycogen content was significantly reduced in the mutant mice (Fig. 3G), consistent with hepatic insulin resistance.

It has been reported that Mstn treatment of wild-type (WT) mice stimulates gluconeogenesis in the liver (*24*). We therefore speculated that the elevated plasma Mstn levels caused by adipocyte barr1 deficiency may promote HGP. To test this hypothesis, we performed a pyruvate tolerance test (PTT), a test that is frequently used to monitor hepatic gluconeogenesis in vivo. In this test, HFD adipo-barr1-KO mice showed significantly more pronounced increases in blood glucose levels as compared to their control littermates (Fig. 3H), suggesting that hepatic gluconeogenesis is increased in the barr1 mutant mice. Consistent with this observation, the expression levels of key gluconeogenic genes (*G6p1*, *Pck1*, and *Pdk4*) were significantly up-regulated in liver RNA from HFD adipo-barr1-KO mice (Fig. 3I). Likewise, the expression of *Tnfa* and *Mip1b* (genes encoding proinflammatory cytokines) was markedly elevated in liver RNA from HFD adipo-barr1-KO mice (Fig. 3I). Liver weight was also increased in the HFD barr1 mutant mice (Fig. 3J), most likely due to enhanced lipid deposition, as indicated by hematoxylin and eosin (H&E) and Oil Red O staining studies (Fig. 3K). In summary, these data clearly indicate that the lack of barr1 in adipocytes caused hepatic insulin resistance.

Barr1 deficiency in BAT increases the expression of myogenic and proinflammatory cytokine genes

We next studied changes in gene expression levels in BAT of adipo-barr1-KO mice and control mice maintained on a HFD for at least 8 weeks. We subjected BAT RNA obtained from both groups of mice to RNA sequencing (RNA-seq) analysis. This analysis identified ~300 genes that were differentially regulated (cutoff: $\log_2$ fold change ≥ 1) (Fig. 4, A and B). The HFD barr1 mutant mice showed increased expression of various myogenic genes including *Myh4*, *Tnnt3*, *Actn3*, *Myh3*, and *Asb15* (Fig. 4A). *Mstn* expression was also markedly increased in BAT from the HFD barr1 mutant mice (Fig. 4A). Ingenuity pathway analysis indicated that the pathways showing the most pronounced changes in gene expression were related to "skeletal muscle function and development" (Fig. 4B). qRT-PCR studies confirmed that barr1 deficiency in BAT markedly increased the expression of *Mstn* and various myogenic genes (Fig. 4, C to E). In contrast, *Mstn* expression levels remained very low in iWAT and eWAT of HFD barr1 mutant and control mice (Fig. 4C).

Moreover, the expression of genes coding for proinflammatory cytokines [TNFα, interferon-γ, MCP1, macrophage inflammatory protein 1A (MIP1A), MIP1B, and interleukin-6 (IL-6)] was significantly up-regulated in BAT from HFD barr1 mutant mice (Fig. 4F). We observed a similar pattern with iWAT and eWAT prepared from HFD adipo-barr1-KO mice (fig. S4, A and B). BAT expression levels of genes involved in adipogenesis and mitochondrial function were not affected by the lack of barr1, except for *Ucp1* expression that was slightly increased (by ~1.7-fold) in BAT lacking barr1 (fig. S4, C and D). Analysis of iWAT RNA showed that barr1 deficiency had no significant effect on the expression of lipogenic genes but caused significant decreases in the expression of genes critical for mitochondrial function (fig. S4, E and F). RNA from eWAT lacking barr1 showed increased *Ppara* and *Ap2* transcript levels but unaltered expression of genes important for mitochondrial function (fig. S4, G and H). Together, these data indicate that barr1 deficiency has pronounced effects on gene expression profiles in different fat depots.

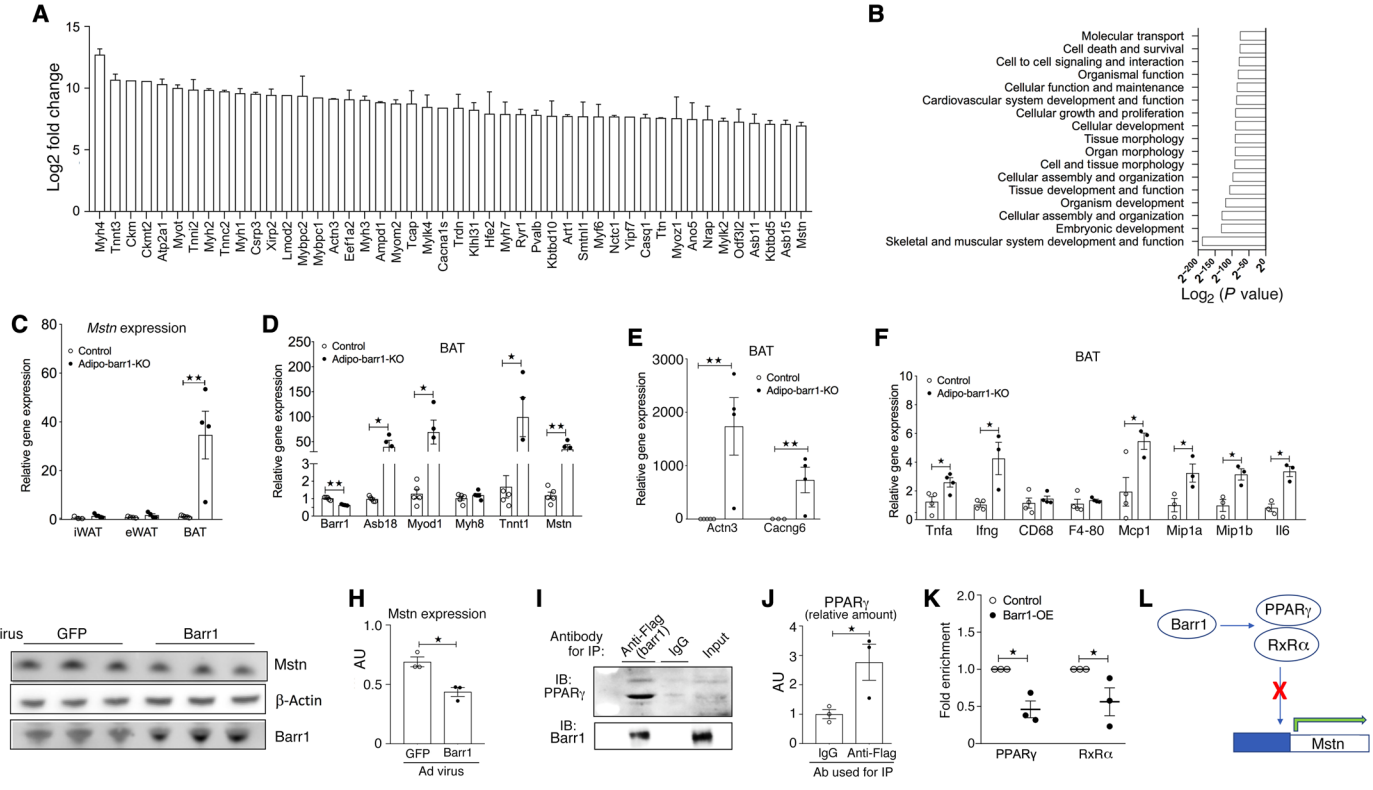

Fig. 4. Adipocyte barr1 deficiency causes increased expression of Mstn and myogenic and proinflammatory genes in BAT. All studies were performed with male mice maintained on a HFD for at least 8 weeks. (**A**) RNA-seq studies showing highly up-regulated genes (top 46) in BAT of HFD adipo-barr1-KO mice (as compared to BAT from HFD control littermates). (**B**) List of highly regulated pathways in BAT from HFD adipo-barr1-KO (as compared to BAT from HFD control littermates). (**C**) *Mstn* gene expression in iWAT, eWAT, and BAT of HFD adipo-barr1-KO and control mice, as determined by qRT-PCR. (**D** and **E**) Transcript levels of myogenic genes in BAT (HFD mice; qRT-PCR). (**F**) Expression levels of proinflammatory cytokine genes in BAT (HFD mice; qRT-PCR). (**G** and **H**) Western blot analysis of Mstn, β-actin, and barr1 expression in a mouse BAT cell line treated with adenoviruses encoding GFP (control) or barr1, respectively. Panel (H) shows a quantification of the immunoblotting data shown in (G). Mstn expression was normalized to that of β-actin. (**I**) Co-immunoprecipitation (co-IP) of barr1 with PPARγ in a mouse BAT cell line. Barr1-Flag was immunoprecipitated from cell lysates with an anti-Flag antibody, followed by immunoblotting studies to detect co-IP PPARγ. "Input" corresponds to cell lysate that was loaded directly onto the gel (1 of 100 of the amount used for co-IP). IB, immunoblot. (**J**) Quantification of the co-IP data shown in (I). The data shown are from three independent co-IP experiments. Relative amounts of co-IP PPARγ are shown. AU, arbitrary units. (**K**) Chromatin immunoprecipitation assay showing fold enrichment of PPARγ and retinoid X receptor α (RXRα) in mouse BAT cells overexpressing barr1 or green fluorescent protein. (**L**) Scheme showing the likely mechanism by which barr1 suppresses *Mstn* expression. All data are expressed as means ± SEM ($n = 3$ to 5). *$P < 0.05$ and **$P < 0.01$ (two-tailed Student's t test).

Since *Ucp1* gene expression was increased by ~1.7-fold in BAT of HFD barr1-KO mice as compared to BAT from HFD control littermates (fig. S4D), we carried out additional studies to explore whether this increase in *Ucp1* expression resulted in altered BAT function. Specifically, we injected HFD adipo-barr1-KO mice and control littermates with CL316,243, a β3-adrenergic receptor–selective agonist. Previous work has shown that the ability of CL316,243 to efficiently increase TEE/O_2 consumption rate in mice requires the presence of BAT β3 receptors and UCP1 (uncoupling protein 1) [see, for example, (*25*)]. We found that CL316,243 treatment of HFD adipo-barr1-KO and control mice caused comparable increases in TEE (fig. S5A). We obtained similar findings when we exposed the mutant and control animals to cold temperatures, a well-known stimulus for BAT thermogenesis (fig. S5B). These observations indicate that the increase in *Ucp1* expression displayed by BAT lacking barr1 did not lead to significant changes in BAT function.

We also noted that the *Ucp1* expression was reduced by ~50% in iWAT of HFD barr1-KO mice as compared to HFD control littermates (fig. S4F). Since the expression of *Ucp1* is very low in iWAT of lean or obese mice (unless mice are exposed to stimuli leading to the "beiging" of white fat) (*26*), it is unlikely that the decreased *Ucp1* expression in iWAT resulted in any notable metabolic changes.

Mstn expression is regulated by interaction of barr1 with PPARγ

The observation that inactivation of *barr1* in adipocytes greatly enhanced *Mstn* expression in BAT was particularly intriguing. To explore the molecular mechanism underlying this finding, we used a barr1-encoding adenovirus to overexpress barr1 in differentiated mouse BAT cells derived from immortalized brown pre-adipocytes (*27*). We found that BAT cells overexpressing barr1 showed significantly reduced Mstn protein levels as compared to BAT cells infected with a green fluorescent protein (GFP)–encoding control adenovirus (Fig. 4, G and H), confirming that barr1 exerts an inhibitory effect on Mstn expression in BAT.

Several studies suggest that nuclear barr1 plays a role in regulating gene transcription (*18*, *28*, *29*). On the basis of our findings, we hypothesized that barr1 may inhibit the transcriptional activity of the *Mstn* promoter. To test this hypothesis, we first screened the *Mstn* gene promoter region for potential transcription factor binding sites. By using the PROMO program (*30*), we identified a potential peroxisome proliferator–activated receptor γ (PPARγ) binding motif in the mouse *Mstn* promoter region (positions −936 to −924). To examine whether nuclear barr1 can interact with PPARγ in brown adipocytes, we isolated nuclei from cultured mouse BAT cells (*27*) overexpressing a Flag-tagged version of barr1. Nuclear extracts were then incubated with either an anti-Flag monoclonal antibody or immunoglobulin G (IgG) (for control purposes). Immunoprecipitated proteins were probed via Western blotting for the presence of PPARγ. This analysis demonstrated that barr1 could be co-immunoprecipitated (co-IP) as a complex with PPARγ (Fig. 4, I and J).

We also performed chromatin immunoprecipitation (ChIP) assays to examine whether barr1 could inhibit the binding of the PPARγ/retinoid X receptor α (RXRα) complex to the *Mstn* promoter. As shown in Fig. 4K, adenovirus-mediated overexpression of barr1 in differentiated mouse BAT cells decreased the binding of PPARγ and RXRα to the promoter region of *Mstn* as compared to control cells (BAT cells infected with an adenovirus encoding GFP). Together, our data indicate that barr1 interacts with the PPARγ/RXRα complex in brown adipocytes, thus interfering with the ability of PPARγ to bind to and stimulate transcription from the *Mstn* promoter (Fig. 4L).

Short-term Mstn treatment impairs insulin signaling in skeletal muscle, adipose tissues, and liver

To examine the effect of elevated plasma Mstn levels on peripheral insulin resistance in a more direct fashion, we treated WT C57BL/6NTac mice maintained on a HFD with either Mstn [0.5 μg/day, subcutaneously (sc)] or phosphate-buffered saline (PBS) for three consecutive days (one injection per day). Four hours after the last Mstn/PBS injection, mice were treated with insulin [5 U, intravenously (iv)], and adipose, skeletal muscle, and liver tissues were collected 5 min later. Western blotting studies showed that Mstn-treated mice showed a significant reduction in insulin-stimulated phosphorylation of AKT (T308 and S473) in iWAT and BAT as compared to PBS-injected control mice (Fig. 5A). This effect was most pronounced in BAT where only residual insulin signaling could be detected after Mstn treatment (Fig. 5A). Mstn-induced inhibition of insulin signaling was also observed in skeletal muscle tissues and hepatocytes of the liver (Fig. 5, B to D).

We also examined whether Mstn treatment of HFD WT mice for 3 days (see previous paragraph) affected the expression of genes encoding myogenic factors/proteins and proinflammatory cytokines and genes critical for mitochondrial function. In iWAT, Mstn treatment stimulated the expression of various genes coding for proinflammatory cytokines including IL-6, TNFα, MCP1, MIP1A, and MIP1B (Fig. 5E). The expression of *Cacng6* and *Ucp1* was also up-regulated in iWAT (Fig. 5E). In eWAT, gene expression levels remained largely unaffected after Mstn treatment (Fig. 5F). In BAT, Mstn treatment enhanced the expression of most myogenic genes studied (*Actn3*, *Asb18*, *Cacng6*, *Myod1*, and *Tnn1*) (Fig. 5G). Mstn treatment also increased the expression levels of several proinflammatory cytokines in BAT, liver, and gastrocnemius muscle (Fig. 5, G to I), but not in quadriceps muscle (Fig. 5J). Together, these data indicate that Mstn inhibits insulin signaling and increases the expression of proinflammatory cytokines in adipose tissue, skeletal muscle (gastrocnemius muscle), and liver. In addition, Mstn promotes the expression of myogenic genes in BAT.

Chronic treatment of HFD adipo-barr1-KO mice with an anti-Mstn antibody improves glucose homeostasis

Since the lack of barr1 in adipocytes led to elevated plasma Mstn levels (Figs. 1K and 2M), we examined the potential contribution of Mstn to the metabolic deficits displayed by the HFD adipo-barr1-KO mice. Specifically, we injected HFD adipo-barr1-KO mice and their control littermates with an anti-Mstn antibody (Mstn-AB; 9 mg/kg, ip) or IgG (9 mg/kg, ip), once a week for a period of 4 weeks (Fig. 6A). This antibody has been shown to bind to Mstn with exquisite selectivity (Acceleron Pharma, Inc.). During the 4-week period, mice continued to consume the HFD. Intraperitoneal glucose tolerance test (IGTT) and insulin tolerance test (ITT) studies were performed after the second and third round of antibody injections, respectively. As expected, the IgG-injected HFD barr1 mutant mice showed a marked impairment in glucose tolerance (Fig. 6B; also see Fig. 2C). Notably, this metabolic deficit was abolished after treatment of the mutant mice with the Mstn-AB (Fig. 6B). Similarly, Mstn-AB treatment restored normal insulin sensitivity to the HFD adipo-barr1-KO mice (Fig. 6C). IgG-treated barr1 mutant mice showed elevated blood glucose, plasma insulin, and

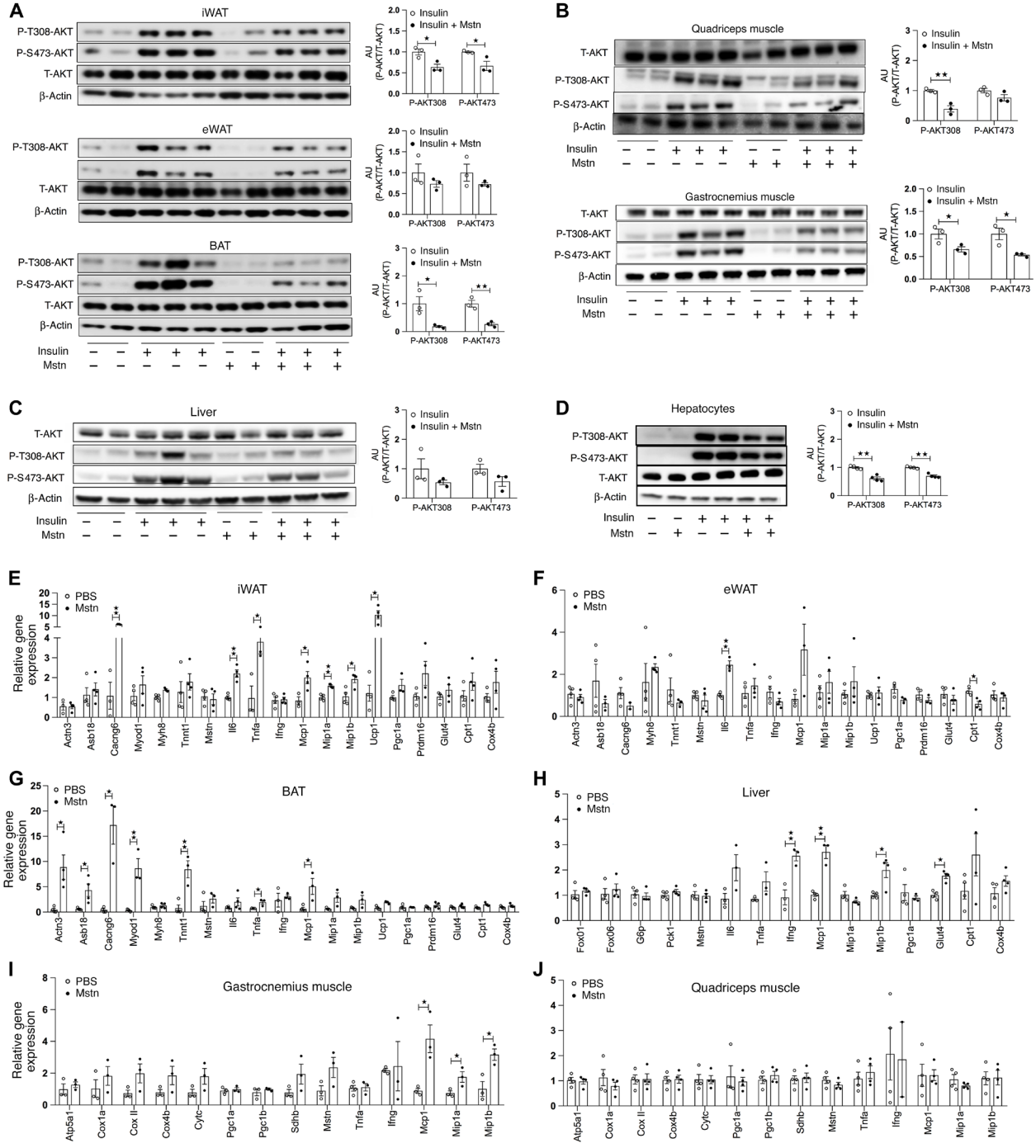

Fig. 5. Mstn impairs insulin signaling and gene expression in skeletal muscle, adipose tissue and liver of HFD WT mice. (**A** to **C**) Effect of short-term Mstn treatment on insulin receptor signaling in various peripheral tissues studied by Western blotting. WT mice (male C57BL/6NTac mice) maintained on an HFD for 6 weeks were injected once a day with Mstn (0.5 μg per mouse, sc) or PBS ("-") for the last 3 days of HFD feeding. Four hours after the last injection, mice received a single dose of insulin (5 U, iv) or vehicle (PBS). Tissues were collected 5 min later, followed by Western blotting studies. Insulin signaling was monitored in BAT, iWAT, and eWAT (A); quadriceps and gastrocnemius muscle (B); and liver (C). (**D**) Effect of Mstn treatment on insulin signaling in primary WT mouse hepatocytes. Hepatocytes were incubated with 10 μM Mstn for 16 hours, followed by treatment with 100 nM insulin for 5 min. In (A) to (D), the outcome of the Western blotting studies is summarized by bar plots. (**E** to **J**) Expression levels of metabolically important genes in BAT, iWAT, eWAT, quadriceps and gastrocnemius muscles, and liver in Mstn-treated HFD WT mice. Mice were treated with Mstn as indicated in (A) to (C). Tissues were collected 4 hours after the last Mstn injection. All data are expressed as means ± SEM ($n = 3$ to 5 male mice per group). *$P < 0.05$ and **$P < 0.01$ (two-tailed Student's t test).

plasma FFA levels (Fig. 6, D to F; also see Fig. 2, F to H) as compared with IgG-treated control littermates. In contrast, after Mstn-AB treatment, barr1 mutant mice showed blood glucose, plasma insulin, and plasma FFA levels that were similar to those obtained with their control littermates (Fig. 6, D to F). These data strongly support the concept that increased plasma Mstn levels play a key

role in causing the metabolic deficits resulting from adipocyte barr1 deficiency.

Overexpression of barr1 in adipocytes improves glucose homeostasis in obese mice

Since inactivation of *barr1* in adipocytes caused severe metabolic deficits, we speculated that overexpression of barr1 in adipocytes may have beneficial effects on whole-body glucose homeostasis. To test this hypothesis, we generated a transgenic mouse line that overexpressed a hemagglutinin (HA)–tagged version of barr1 in adipose tissue under the transcriptional control of the adiponectin promoter (fig. S6A). For simplicity, we refer to these mice as "adipo-barr1-OE mice."

Adipo-barr1-OE mice and WT littermates maintained on RC showed no significant differences in body weight, glucose tolerance, insulin sensitivity, and blood glucose, plasma insulin, and plasma FFA levels (fig. S6, B to G). We next carried out experiments with adipo-barr1-OE mice and WT littermates consuming an obesogenic HFD. The HFD-induced gain in body weight was comparable between the two groups of mice (Fig. 7A). Similarly, magnetic resonance imaging (MRI) studies revealed no significant differences in body composition (lean versus fat mass) (Fig. 7B). Notably, the HFD adipo-barr1-OE mice displayed pronounced improvements in glucose tolerance and insulin sensitivity (Fig. 7, C and D). Moreover, in a PTT, the mutant mice showed significantly smaller blood glucose excursions than their WT littermates (Fig. 7E). Blood glucose and plasma insulin and FFA levels were significantly decreased in the HFD adipo-barr1-OE mice (Fig. 7, F to H). In contrast to HFD adipo-barr1-KO mice that displayed elevated plasma Mstn levels (Figs. 1K and 2M), HFD adipo-barr1-OE mice showed a significant reduction in plasma Mstn levels (Fig. 7I). Collectively, these data indicate that overexpression of barr1 in adipocytes protects mice from obesity-associated metabolic deficits.

Mstn treatment reverses the metabolic improvements displayed by HFD adipo-barr1-OE mice

We next examined whether the reduced plasma Mstn levels displayed by the adipo-barr1-OE mice contributed to the metabolic improvements caused by overexpression of barr1 in adipocytes. Specifically, we injected HFD adipo-barr1-OE mice and their WT littermates with either Mstn (0.5 μg, sc) or PBS (two injections administered 24 and 4 hours before metabolic tests; Fig. 7J). Before metabolic testing, all groups of mice showed similar body weight (Fig. 7K). Consistent with the data shown in Fig. 7F, PBS-treated adipo-barr1-OE mice showed significantly lower blood glucose levels than their

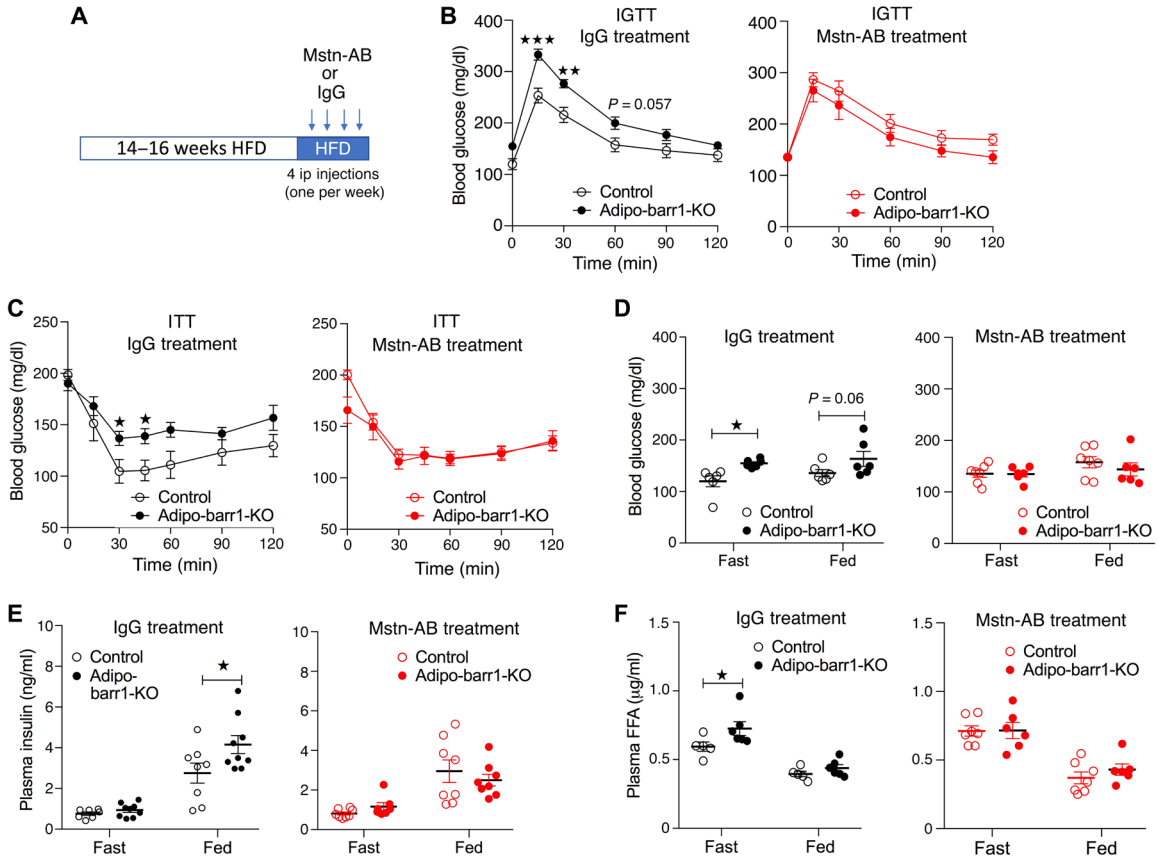

Fig. 6. Chronic treatment of HFD adipo-barr1-KO mice with an anti-Mstn antibody restores normal glucose and insulin tolerance. All studies were performed with HFD adipo-barr1-KO and control mice (males). (**A**) Study design. Adipo-barr1-KO and control mice that had been maintained on HFD for 14 to 16 weeks were injected with an anti-Mstn antibody (Mstn-AB; 9 mg/kg, ip) or IgG (for control purposes) once a week for a period of 4 weeks (four injections total). Metabolic tests were performed after the second (IGTT) and third (ITT) injection, respectively. (**B**) IGTT (1 g of glucose per kilogram, ip). (**C**) ITT (0.75 U/kg, ip). (**D**) Fasting and fed blood glucose levels. (**E**) Fasting and fed plasma insulin levels. (**F**) Fasting and fed plasma FFA levels. All data are expressed as means ± SEM ($n = 6$ to 8). $^{\star}P < 0.05$, $^{\star\star}P < 0.01$, $^{\star\star\star}P < 0.001$ [(B and C) two-way ANOVA followed by Bonferroni's post hoc test; (D to F) two-tailed Student's *t* test].

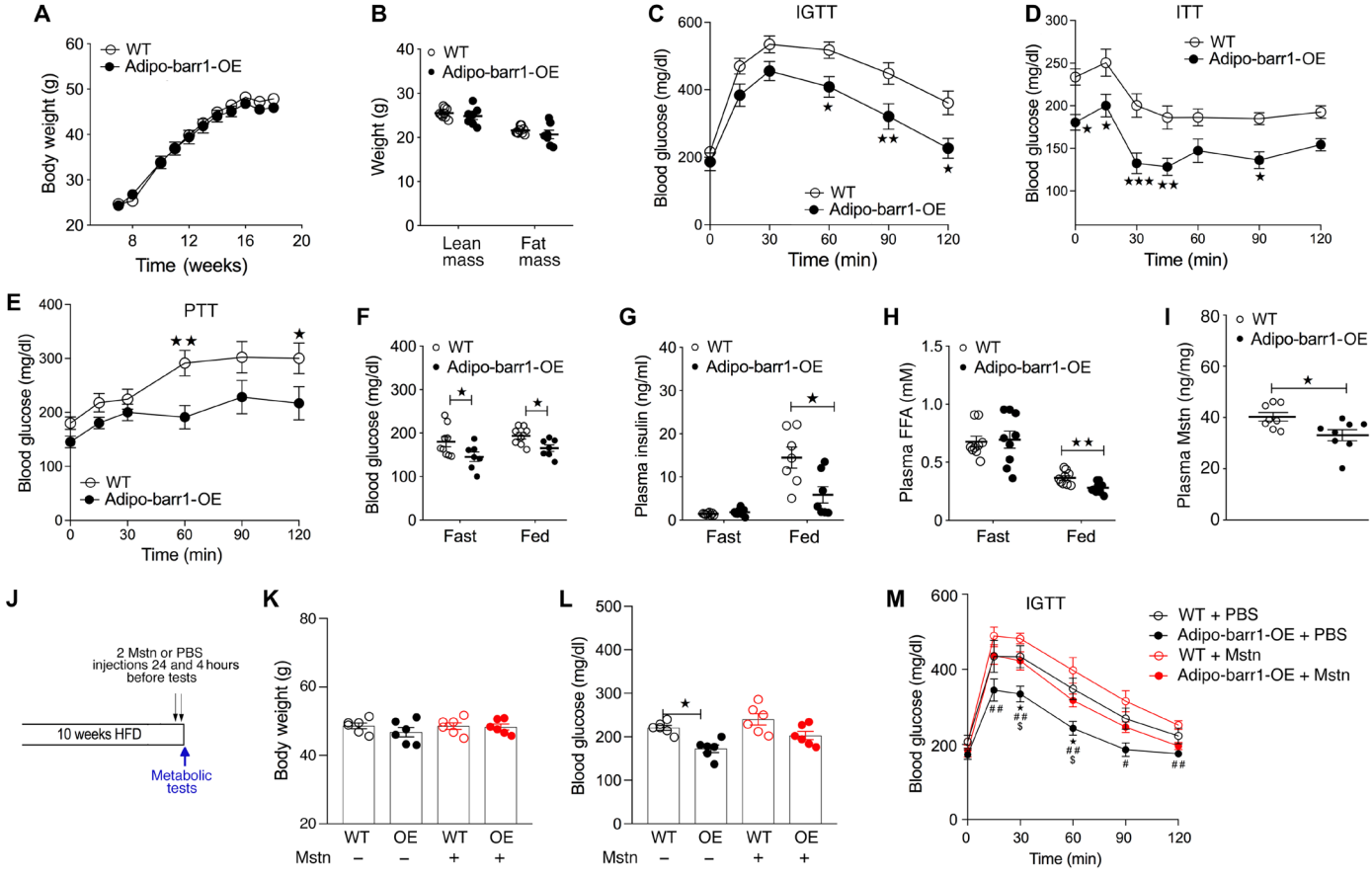

Fig. 7. Metabolic studies with HFD mice overexpressing barr1 in adipocytes. All experiments were carried out with adipo-barr1-OE mice and WT littermates (males) that had been maintained on a HFD for at least 8 weeks. (**A**) Body weights of adipo-barr1-OE mice and WT littermates consuming a HFD. (**B**) Body composition (lean versus fat mass) of mice maintained on a HFD for 11 weeks. (**C**) GTT (1 g of glucose per kilogram, ip). (**D**) ITT (0.75 U/kg, ip). (**E**) PTT (2 g of pyruvate per kilogram, ip). (**F** and **G**) Fasting and fed blood glucose (F) and plasma insulin (G) levels. (**H**) Fasting and fed plasma FFA levels. (**I**) Plasma Mstn levels. Measurements were taken at 10 a.m. (**J**) Experimental design. Adipo-barr1-OE mice and WT littermates were maintained on HFD for 10 weeks and received two doses of Mstn (0.5 μg, sc) or PBS 24 and 4 hours before metabolic tests. (**K**) Body weights of Mstn- and PBS-injected mice. (**L**) Blood glucose levels after injection of Mstn or PBS. (**M**) IGTT (1 g of glucose per kilogram, ip) after injection of Mstn or PBS. Data represent means ± SEM ($n = 6$ to 9). $^*P < 0.05$, $^*P < 0.01$, $\#P < 0.05$, $\#\#P < 0.01$, and $\$P < 0.05$ [(C to E) and (L) two-way ANOVA followed by Bonferroni's post hoc test; (F to I) two-tailed Student's *t* test; (M) Dunnett's test for multiple comparisons; adipo-barr1-OE + PBS versus WT + PBS (*), adipo-barr1-OE + PBS versus WT + Mstn (# or ##), and adipo-barr1-OE + PBS versus adipo-barr1-OE + Mstn ($)].

WT littermates (Fig. 7L). In contrast, Mstn-treated mutant mice showed similar blood glucose levels as Mstn-treated WT mice (Fig. 7L). As expected, PBS-treated adipo-barr1-OE mice showed improved glucose tolerance when compared to PBS-treated WT littermates (Fig. 7M; see also Fig. 7C). This improvement in glucose tolerance was no longer observed with Mstn-treated adipo-barr1-OE mice (Fig. 7M). These observations indicate that barr1 regulation of plasma Mstn levels is required for the maintenance of euglycemia.

DISCUSSION

The two β-arrestins (barr1 and barr2) are intracellular proteins that play a key role in GPCR desensitization and internalization (*12*, *13*). However, it is now generally accepted that both proteins can also act as signaling proteins in their own right (*14*–*16*). For example, it has been reported that nuclear barr1 plays a role in regulating gene transcription (*18*, *28*, *29*).

Several studies have shown that barr1/2 modulates many important metabolic functions (*10*, *31*–*33*). In the present study, we report the unexpected observation that mice lacking barr1 selectively in adipocytes (adipo-barr1-KO mice) showed severely impaired glucose tolerance and insulin sensitivity when consuming an obesogenic diet. On the other hand, transgenic mice that overexpressed barr1 in adipocytes (adipo-barr1-OE mice) were protected against the metabolic deficits caused by a high-calorie diet.

To explore the cellular mechanisms underlying these phenotypes, we studied gene expression patterns in the three major fat depots, iWAT, eWAT, and BAT. The most notable changes in gene expression were observed with BAT lacking barr1 (Fig. 4, A to F). qRT-PCR and RNA-seq studies showed that the expression of most myogenic genes was greatly enhanced in BAT derived from adipo-barr1-KO mice (Fig. 4, A to E). We found that the expression of *Mstn* was markedly increased in BAT of adipo-barr1-KO mice (Figs. 1I and 4C). In contrast, *Mstn* expression was not affected by the barr1 mutation in iWAT, eWAT, or skeletal muscle tissues (Fig. 1I). BAT precursor cells originate from a *Myf5*-positive lineage (*34*–*36*), which can give rise to either myocytes or brown adipocytes,

explaining why genetic manipulation of BAT cells can lead to a myogenic gene expression profile.

Mstn, a member of the transforming growth factor–β superfamily, is best known for its ability to inhibit skeletal muscle growth (*37*, *38*). However, accumulating evidence suggests that Mstn has also important skeletal muscle–independent functions. For example, it has been demonstrated that Mstn can act as a negative regulator of brown adipocyte differentiation (*39*, *40*).

In the present study, the lack of barr1 in BAT caused a myogenic gene expression profile, including a pronounced increase in BAT Mstn expression and elevated plasma Mstn levels (Figs. 1K and 2M). In contrast, adipo-barr1-OE mice displayed reduced plasma Mstn levels (Fig. 7I). To explore whether altered plasma Mstn levels were responsible, at least in part, for the impairments in glucose tolerance and insulin sensitivity observed with the adipo-barr1-KO mice, we treated HFD adipo-barr1-KO mice with an Mstn-AB. Notably, Mstn-AB treatment corrected all metabolic deficits caused by the barr1 mutation, leading to greatly improved glucose tolerance and insulin sensitivity, and normal blood glucose, plasma insulin, and plasma FFA levels (Fig. 6). In a related set of experiments, we treated HFD adipo-barr1-OE mice, which showed reduced plasma Mstn levels and improved glucose tolerance (as compared with HFD control littermates), with Mstn. While Mstn administration did not cause any changes in body weight, it virtually abolished the improvements in glucose homeostasis caused by overexpression of barr1 in adipocytes (Fig. 7, L and M). Together, these data support the concept that barr1 suppresses Mstn expression in BAT and that reduction or enhancement of BAT barr1 levels triggers changes in plasma Mstn levels that have a major impact on whole-body glucose homeostasis.

To study the metabolic effects of Mstn in greater detail, we injected WT mice for 3 days with Mstn (one injection per day). We found that Mstn treatment increased the expression of many myogenic genes in mouse BAT (Fig. 5G), suggesting that the myogenic gene expression signature observed with BAT lacking barr1 was caused by enhanced Mstn expression. In addition, Mstn treatment of HFD WT mice led to impaired insulin signaling in iWAT, BAT, skeletal muscle tissues, and hepatocytes (Fig. 5, A, B, and D), associated with increased expression levels of genes encoding proinflammatory cytokines such as MCP1, IL-6, and TNFα in these tissues (Fig. 5, E to I). These observations are in agreement with the notion that the metabolic impairments observed with the adipo-barr1-KO mice were primarily caused by Mstn-mediated deficits in insulin signaling in the major insulin target tissues.

In addition to enhanced *Mstn* expression, BAT from HFD adipo-barr1-KO mice also showed a significant increase in the expression of genes coding for proinflammatory cytokines (Fig. 4F). In contrast, transcript levels of BAT genes involved in adipogenesis and mitochondrial function remained unaffected by the lack of barr1, except for a slight increase in *Ucp1* expression (fig. S4, C and D). Since Mstn treatment of obese WT mice promoted the expression of proinflammatory cytokines and impaired insulin signaling in BAT (Fig. 5, A and G), it is likely that Mstn released from BAT cells acts in an autocrine fashion to cause similar effects/deficits in BAT from HFD adipo-barr1-KO."

HFD adipo-barr1-KO mice showed decreased hepatic glycogen content (Fig. 3G), enhanced glucose excursions in a pyruvate tolerance test (Fig. 3H), and elevated expression levels of key gluconeogenic genes (Fig. 3I), suggesting that impaired insulin signaling is the primary cause of the increase in hepatic gluconeogenesis displayed by the mutant mice. In agreement with this concept, Ji *et al.* (*41*) demonstrated that Mstn-induced signaling can inhibit PI3 kinase by activating PTEN, thus interfering with insulin receptor signaling.

Two recent studies also reported that Mstn release from BAT can result in altered metabolic functions. Steculorum *et al.* found that stimulation of hypothalamic AgRP neurons can promote the expression of myogenic genes in mouse BAT, including increased expression of Mstn (*23*). These authors also demonstrated that inhibition of Mstn activity improved insulin sensitivity that was impaired following the stimulation of AgRP neurons. In another study, Kong *et al.* (*22*) showed that inactivation of the transcription factor interferon regulatory factor 4 (IRF4) in BAT reduces exercise capacity in mice and that this phenotype is most likely caused by increased myogenic gene expression in BAT, including enhanced Mstn expression and secretion.

Barr1 (but not barr2) has been shown to interact with various transcription factors in the nucleus, thus regulating gene transcription (*18*, *28*, *29*). In the present study, we demonstrated that barr1 is able to bind to PPARγ in nuclear extracts prepared from differentiated mouse BAT cells (Fig. 4, I and J). Moreover, ChIP assays strongly suggested that the interaction of barr1 with PPARγ prevents binding of PPARγ to the promoter region of the *Mstn* gene (Fig. 4K). These findings provide a molecular basis for the observation that the lack of barr1 in BAT promotes the expression of Mstn (Fig. 4L).

Consistent with our findings, Kang *et al.* (*18*) demonstrated that barr1 can interact with PPARγ and negatively regulate the transcriptional activities of PPARγ in the nucleus. In a follow-up study, Zhuang *et al.* (*42*) showed that the interaction of barr1 with PPARγ inhibited the formation of a PPARγ/RXRα heterodimer, thus enhancing the formation of a PPARγ/nuclear receptor corepressor repressive complex (*42*). A more recent study demonstrated that barr1 binding to PPARγ (as well as to PPARα) requires the presence of a LXXXLXXXL motif in barr1 and that this interaction can regulate BAT function (*43*).

Genetic deletion of Mstn in mice caused increased muscle mass and improved insulin sensitivity in HFD mice (*44*–*46*). A similar pattern was observed in rat, pig, and cattle (*47*). On the other hand, overexpression of Mstn in mouse skeletal muscle resulted in a notable decrease in muscle mass (*48*). In the present study, adipo-barr1-KO and adipo-barr1-OE mice displayed altered plasma Mstn levels but did not show any significant changes in lean mass as compared to their respective control groups. This observation is consistent with the outcome of a recent study where deletion of IRF4 from mouse adipocytes increased serum Mstn levels but did not affect lean mass (*22*). As suggested by Kong *et al.* (*22*), it is likely that the relatively modest changes in plasma Mstn levels displayed by the mutant mouse strains analyzed in this study do not suffice to trigger notable changes in muscle mass.

In a previous study, we demonstrated that mice selectively lacking barr2 in adipocytes (adipo-barr2-KO mice) show pronounced improvements in glucose homeostasis (*10*), a phenotype that is exactly opposite to the one observed in the present study with adipo-barr1-KO mice. We found that these beneficial metabolic effects were primarily due to enhanced signaling via adipocyte β3-adrenergic receptors (*10*). Thus, the notably different phenotypes of adipo-barr1-KO versus adipo-barr2-KO mutant mice indicate that barr1 and barr2 can have opposing functions in the same cell type in vivo.

In conclusion, our data indicate that barr1 acts an efficient negative regulator of Mstn expression in BAT. By using loss- and

gain-of-function mouse models, we provide convincing evidence that barr1 regulation of Mstn expression in BAT is essential for maintaining euglycemia and proper insulin responsiveness of peripheral tissues. Strategies aimed at enhancing the expression or activity of barr1 in BAT may prove useful to improve glucose homeostasis and insulin sensitivity in T2D.

MATERIALS AND METHODS

Animals

Adipo-barr1-KO mice were generated as follows. *Adipoq-Cre* mice were purchased from the Jackson laboratory (stock no. 010803; genetic background: C57BL/6J). *barr1 f/f* mice on a C57BL/6J background were provided by R. Lefkowitz (Duke University, Durham, NC) (*20*). *Barr1 f/f* mice were crossed with *adipoq-Cre* mice to generate adipo-barr1-KO mice and *barr1 f/f* control littermates.

A transgenic mouse line overexpressing barr1 in adipose tissue was generated by using standard transgenic techniques. Plasmid DNA coding for an HA-tagged version of barr1 (Addgene no. 14687) was used to generate a construct in which barr1 expression was under the transcriptional control of the adiponectin promoter. The linearized transgene construct was microinjected into the pronuclei of ova prepared from C57BL/6NTac mice (Taconic). We identified a transgenic line that selectively overexpressed barr1 in adipocytes (adipo-barr1-OE mice). This mouse line was maintained on a pure C57BL/6NTac background. All animal studies were carried out according to the U.S. National Institutes of Health Guidelines for Animal Research and were approved by the National Institute of Diabetes and Digestive and Kidney Diseases Institutional Animal Care and Use Committee.

Mouse maintenance and diet

All experiments were performed with adult male mice, unless stated otherwise. Mice were kept on a 12-hour light and 12-hour dark cycle. Animals were maintained at room temperature (23°C) on standard chow (7022 NIH-07 diet, 15% kcal fat, energy density of 3.1 kcal/g; Envigo Inc). Mice had free access to food and water. In a subset of experiments, mice that were at least 8 weeks old were switched to an HFD (F3282, 60% kcal fat, energy density of 5.5 kcal/g; Bioserv). Mice consumed the HFD for at least 8 weeks, unless stated otherwise.

RNA extraction and qRT-PCR studies

Mice were euthanized, and tissues were collected and frozen quickly on dry ice. Total RNA was extracted using the RNeasy Mini Kit (Qiagen). SuperScript III First-Strand Synthesis SuperMix (Invitrogen) was used to synthesize complementary DNA, and qRT-PCR studies were performed using the SYBR Green method (Applied Biosystems) as described (*49*). Gene expression data were normalized to the expression of 18*S* ribosomal RNA using the ΔΔCt method. A complete list of primer sequences is provided in table S1.

In vivo metabolic tests

Mice that were used for metabolic tests were at least 8 weeks old. For IGTT, mice were fasted for 4 or 12 hours (overnight), as indicated. After treatment of mice with glucose (1 or 2 g/kg), blood glucose levels were measured at regular intervals (0, 15, 30, 60, 90, and 120 min) using a portable glucometer (Contour Glucometer, Bayer). For ITT, mice were fasted for 4 to 5 hours and then injected intraperitoneally with human insulin (0.75 or 1 U/kg; Humulin, Eli Lilly). For PTT, mice were fasted 4 to 5 hours, followed by the administration of sodium pyruvate (2 g/kg, ip). Blood glucose levels were measured at defined time points after the administration of insulin (ITT) or pyruvate (PTT).

Measurement of plasma insulin, leptin, and Mstn levels

Plasma insulin and leptin levels were measured using plasma prepared from mice that had free access to food (fed mice) or from mice that had been fasted overnight for 12 to 14 hours (fasted mice). Blood was collected from the tail vein and centrifuged at 4°C for 10 min at ~12,000*g* to obtain plasma. Plasma insulin, leptin, and Mstn levels were measured using enzyme-linked immunosorbent assay kits from Crystal Chem Inc. (insulin) or R&D Systems (leptin and Mstn), following the manufacturer's instructions.

Determination of plasma cytokine and adipokine levels

Plasma adipokine and cytokine levels were measured using plasma from mice that had been maintained on a HFD for at least 8 weeks. Blood was obtained from the mandibular/jugular vein and collected in K_2-EDTA–containing tubes (Microvette, Sarstedt). Blood samples were centrifuged at 4°C for 10 min at ~12,000*g* to obtain plasma. Cytokine/adipokine levels were measured using the Bio-Plex Multiplex Immunoassay System (Bio-Rad), following the manufacturer's instructions.

Intravenous injection of insulin

Mice that had been fasted for 4 hours were deeply anesthetized with isoflurane. Subsequently, mice were injected into the inferior vena cava with 5 U of insulin dissolved in 100 μl of saline (Humulin, Eli Lilly) or 100 μl of saline (control). Five minutes later, adipose, skeletal muscle, and liver tissues were collected and used for Western blotting studies (*50*).

Body composition analysis

Mouse body mass composition (lean versus fat mass) was measured using a 3-in-1 Echo MRI Analyzer (Echo Medical System).

RNA-seq studies

Libraries for RNA-seq studies were prepared as described previously (*10*). Briefly, total RNA was extracted from BAT of adipo-barr1-KO mice and control littermates (males) that had been maintained on an HFD for 8 weeks. RNAs with RNA integrity number of >8 were used for library preparation. The HiSeq 2500 Sequencing System (Illumina) was used to perform high-throughput sequencing. Mouse genome mm9 was used to map the raw data. The Genomatix genome analyzer was used to identify differentially expressed genes. Enrichment analysis and the analysis of biological pathways were performed using MetaCore (version 6.32, Thomson Reuters, NY). The RNA-seq data can be downloaded from the National Center for Biotechnology Information Sequence Read Archive under reference number RNA seq-PRJNA565949.

Indirect calorimetry measurements

TEE, respiratory exchange ratio (O_2 consumed/CO_2 produced), food intake, and locomotor activity (assayed by beam breaks) were measured simultaneously in mice housed at 22°C using an Oxymax/CLAMS (Columbus Instruments). Sampling was performed every 13 min, measuring from 12 chambers. Mice were adapted in the chambers for 2 days, and data were collected over a 24-hour period.

Water and food were provided ad libitum (*10*). For testing β3-adrenergic receptor–mediated thermogenesis, mice were maintained at 30°C overnight and then injected intraperitoneally with CL316, 243 [0.1 mg/kg; selective β3-adrenergic receptor agonist (Sigma-Aldrich)] or vehicle (saline) with a crossover treatment performed on the following day. Cold-induced thermogenesis was tested by exposing mice to various temperatures (13°, 16°, 19°, 22°, and 30°C) for 3 hours during the light cycle after 2 days of adaptation to metabolic cages at room temperature.

Isolation of mature adipocytes

The isolation of mature mouse adipocytes was performed as described previously (*10*). Briefly, mouse fat pads were collected and digested with KRH (Krebs-Ringer Bicarbonate) buffer containing collagenase 1 (3 mg/ml). Digested tissues were filtered through a 250-μm cell strainer. After a 5-min centrifugation step at 300 rpm (~40*g*), the top layer containing mature adipocytes was collected and used for further experiments.

H&E and Oil Red O staining experiments

Livers were collected from control and mutant mice maintained on an HFD for 12 weeks. H&E and Oil Red O staining experiments of liver slices were performed using standard techniques.

Tissue glucose uptake in vivo

In vivo tissue glucose uptake studies were carried out with mice maintained on RC. After a 4- to 5-hour fast, mice were injected with insulin (Humulin, 0.75 U/kg, ip) and a trace amount of 2-deoxy-D-[1-^{14}C] glucose (10 μCi; PerkinElmer). Forty minutes later, the mice were euthanized, and tissues were collected, weighed, and homogenized. Radioactivity was measured and counted as described (*51*).

Differentiation of mouse brown pre-adipocytes

Immortalized mouse brown pre-adipocytes (*27*) were plated in collagen-coated 10-cm or six-well plates and maintained in Dulbecco's minimum essential medium (DMEM) supplemented with 10% fetal bovine serum (FBS) in a 5% CO_2 incubator at 37°C. Once cells reached confluency, they were treated with differentiation medium containing dexamethasone (2 μg/ml), 0.5 mM 3-isobutyl-1-methylxanthine, 0.125 mM indomethacin, 20 nM insulin, and 1 nM T3. The medium was then removed, and cells were incubated with DMEM containing 10% FBS, 20 nM insulin, and 1 nM T3 for another 48 hours. After completion of the differentiation process, mature brown adipocytes were used for further studies.

Isolation and culture of primary mouse hepatocytes

WT mice (10- to 12-week-old males; strain: C57BL/6NTac) were anesthetized with tribromoethanol (250 mg/kg, ip), and hepatocytes were isolated using a previously described collagenase perfusion protocol (*52*). Isolated hepatocytes were cultured in DMEM containing 10% FBS in collagen-coated 12-well plates. Once the cells were attached, they were incubated for 16 hours in DMEM in the absence or presence of 10 μM Mstn. The cells were then treated with 100 nM insulin for 5 min, followed by Western blotting studies.

Co-IP assays

The Dynabeads co-IP Kit (Thermo Fisher Scientific) was used to perform co-IP assays. Differentiated mouse brown adipocytes (*27*) were infected with an adenovirus coding for a Flag-tagged version of barr1 [50 multiplicity of infection (MOI), Vector Biolabs) or an adenovirus coding for enhanced GFP (eGFP) (control; 50 MOI, UNC Vector Core). Forty-eight hours later, cells were lysed, and nuclei were collected. Nuclei were then lysed in co-IP lysis buffer supplemented with 100 mM NaCl, 0.1% SDS, and protease inhibitors (Roche). Briefly, anti-Flag antibody or IgG was covalently coupled to the epoxy beads provided by the kit. Following this step, beads were incubated for 30 min at 4°C with nuclear lysates. Protein complexes were eluted in elution buffer containing LDS sample buffer (Thermo Fisher Scientific). Samples were analyzed by Western blotting using anti-PPARγ and anti-barr1 antibodies (see table S2 for details).

ChIP assay

Differentiated mouse brown adipocytes (*27*) were infected with adenoviruses coding for either barr1-flag (Vector Biolabs) or eGFP (control, UNC Vector Core). Two days after infection, cells were fixed with formaldehyde, and ChIP assays were performed using the Abcam ChIP Kit (ab500), following the manufacturer's instructions. Antibodies against PPARγ and RXR1α (see table S2 for details) were used to immunoprecipitate PPARγ- and RXR1α-bound promoter regions. Subsequently, PCR was performed on the eluted DNA using primers annealing to the promoter region of the mouse *Mstn* gene. Primer sequences used for PCR analysis are listed in table S1.

Western blots

Western blot analysis was performed as described previously (*10*). Briefly, tissues per cells were homogenized using adipocyte lysis buffer [50 mM tris (pH 7.4), 500 mM NaCl, 1% NP-40, 20% glycerol, 5 mM EDTA, and 1 mM phenylmethylsulphonyl fluoride], followed by centrifugation at 12,000*g* for 15 min. A bicinchoninic acid assay kit (Pierce) was used to determine protein concentrations. Protein samples were denatured and separated via SDS–polyacrylamide gel electrophoresis, followed by transfer to nitrocellulose membranes. Membranes were then incubated with primary and horseradish peroxidase–conjugated secondary antibodies (see table S2 for details), followed by visualization of immunoreactive bands by using SuperSignal West Pico Chemiluminescent Substrate (Pierce).

Injection of mice with Mstn

WT mice (male C57BL/6NTac mice) maintained on HFD for 6 to 7 weeks were injected subcutaneously for three consecutive days with either Mstn (0.5 μg/day) or PBS (*53*). After the third injection, mice were fasted for 4 hours and injected with 100 μl of 5 U of insulin or PBS into the inferior vena cava. Mice were euthanized 5 min later, and tissues were collected and snap frozen for further analysis.

Anti-Mstn antibody treatment

Adipo-barr1-KO and control mice were maintained on HFD for 12 to 14 weeks and then injected with an Mstn-AB (9 mg/kg, ip) or IgG (9 mg/kg, ip) once a week for a period of 4 weeks (*22*). GTT, ITT, and tissue glucose uptake assays were performed after the second, third, and fourth Mstn-AB/PBS injection, respectively. Assays were carried out ~18 hours after antibody injections (injection time: ~4 p.m.).

Liver glycogen measurements

Livers from control and mutant mice were collected and snap frozen immediately. Hepatic glycogen was measured by using a commercially available kit (Abnova).

Hyperinsulinemic-euglycemic insulin clamp

Adipo-barr1-KO and control mice (males) maintained on HFD for 12 weeks were used for hyperinsulinemic-euglycemic clamp experiments. Catheters were placed into the internal jugular vein and the carotid artery. One week after surgery, mice were used for experiments. On the day of the experiment, mice were fasted for 4 hours before the clamp, and animals were unrestrained and conscious throughout the process. Before the equilibration period (−120 to 0 min), each mouse received a 1.2-μCi bolus of [3-^{3}H]glucose (PerkinElmer), followed by a 0.04 μCi/min infusion of [3-^{3}H]glucose for 2 hours at a pump rate of 1 μl/min (CMA Microdialysis) during the clamp period (0 to 120 min). During the clamp, mice received a continuous infusion of human insulin (3 mU/min per kg; Eli Lilly) at a rate of 0.4 μl/min. Blood glucose levels were measured every 10 min, and euglycemia (blood glucose: 120 to 160 mg/dl) was maintained by adjusting the infusion rate of the mix of 40 μCi [^{3}H]-glucose in 600 μl of 45% glucose (hot glucose infusion or HOT GINF). Steady state was achieved at ~60 to 70 min, and blood samples were collected every 10 min for 80 to 120 min and processed for measuring radioactivity in the blood. Rates of endogenous HGP rate, Rd, Rt, and glycogen synthesis were determined using deproteinized [3-^{3}H]glucose plasma samples (*54*, *55*).

Statistics

Data are expressed as means ± SEM for the indicated number of observations. Statistical significance of the data was assessed by two-way analysis of variance (ANOVA), followed by the indicated post hoc tests or by using a two-tailed unpaired Student's *t* test, as appropriate. A *P* value of less than 0.05 was considered statistically significant. The specific statistical tests that were used are indicated in the figure legends.

SUPPLEMENTARY MATERIALS

Supplementary material for this article is available at http://advances.sciencemag.org/cgi/content/full/6/23/eaba1733/DC1

View/request a protocol for this paper from *Bio-protocol*.

REFERENCES AND NOTES

1. D. W. Lam, D. LeRoith, The worldwide diabetes epidemic. *Curr. Opin. Endocrinol. Diabetes Obes.* **19**, 93–96 (2012).
2. A. Hruby, F. B. Hu, The epidemiology of obesity: A big picture. *Pharmacoeconomics* **33**, 673–689 (2015).
3. P. González-Muniesa, M.-A. Mártinez-González, F. B. Hu, J.-P. Després, Y. Matsuzawa, R. J. F. Loos, L. A. Moreno, G. A. Bray, J. A. Martinez, Obesity. *Nat. Rev. Dis. Primers.* **3**, 17034 (2017).
4. D. P. Guh, W. Zhang, N. Bansback, Z. Amarsi, C. L. Birmingham, A. H. Anis, The incidence of co-morbidities related to obesity and overweight: A systematic review and meta-analysis. *BMC Public Health* **9**, 88 (2009).
5. A. Guilherme, J. V. Virbasius, V. Puri, M. P. Czech, Adipocyte dysfunctions linking obesity to insulin resistance and type 2 diabetes. *Nat. Rev. Mol. Cell Biol.* **9**, 367–377 (2008).
6. C. M. Kusminski, P. E. Bickel, P. E. Scherer, Targeting adipose tissue in the treatment of obesity-associated diabetes. *Nat. Rev. Drug Discov.* **15**, 639–660 (2016).
7. A. R. Saltiel, J. M. Olefsky, Inflammatory mechanisms linking obesity and metabolic disease. *J. Clin. Invest.* **127**, 1–4 (2017).
8. G.-X. Wang, X.-Y. Zhao, Z.-X. Meng, M. Kern, A. Dietrich, Z. Chen, Z. Cozacov, D. Zhou, A. L. Okunade, X. Su, S. Li, M. Blüher, J. D. Lin, The brown fat-enriched secreted factor Nrg4 preserves metabolic homeostasis through attenuation of hepatic lipogenesis. *Nat. Med.* **20**, 1436–1443 (2014).
9. A. Ali Khan, J. Hansson, P. Weber, S. Foehr, J. Krijgsveld, S. Herzig, M. Scheideler, Comparative secretome analyses of primary murine white and brown adipocytes reveal novel adipokines. *Mol. Cell. Proteomics* **17**, 2358–2370 (2018).
10. S. P. Pydi, S. Jain, W. Tung, Y. Cui, L. Zhu, W. Sakamoto, S. Jain, B. S. Abel, M. C. Skarulis, J. Liu, T. Huynh, K. Pacak, M. G. Caron, O. Gavrilova, T. Finkel, J. Wess, Adipocyte β-arrestin-2 is essential for maintaining whole body glucose and energy homeostasis. *Nat. Commun.* **10**, 2936 (2019).
11. L. Wang, S. P. Pydi, Y. Cui, L. Zhu, J. Meister, O. Gavrilova, R. Berdeaux, J.-P. Fortin, K. K. Bence, C. Vernochet, J. Wess, Selective activation of G_s signaling in adipocytes causes striking metabolic improvements in mice. *Mol. Metab.* **27**, 83–91 (2019).
12. K. L. Pierce, R. T. Premont, R. J. Lefkowitz, Seven-transmembrane receptors. *Nat. Rev. Mol. Cell Biol.* **3**, 639–650 (2002).
13. J. G. Krupnick, J. L. Benovic, The role of receptor kinases and arrestins in G protein-coupled receptor regulation. *Annu. Rev. Pharmacol. Toxicol.* **38**, 289–319 (1998).
14. L. M. Luttrell, D. Gesty-Palmer, Beyond desensitization: Physiological relevance of arrestin-dependent signaling. *Pharmacol. Rev.* **62**, 305–330 (2010).
15. S. Rajagopal, K. Rajagopal, R. J. Lefkowitz, Teaching old receptors new tricks: Biasing seven-transmembrane receptors. *Nat. Rev. Drug Discov.* **9**, 373–386 (2010).
16. V. V. Gurevich, E. V. Gurevich, Overview of different mechanisms of arrestin-mediated signaling. *Curr. Protoc. Pharmacol.* **67**, 2.10.1–2.10.9 (2014).
17. A. Srivastava, B. Gupta, C. Gupta, A. K. Shukla, Emerging functional divergence of β-arrestin isoforms in GPCR function. *Trends Endocrinol. Metab.* **26**, 628–642 (2015).
18. J. Kang, Y. Shi, B. Xiang, B. Qu, W. Su, M. Zhu, M. Zhang, G. Bao, F. Wang, X. Zhang, R. Yang, F. Fan, X. Chen, G. Pei, L. Ma, A nuclear function of β-arrestin1 in GPCR signaling: Regulation of histone acetylation and gene transcription. *Cell* **123**, 833–847 (2005).
19. L.-N. Zhuang, W.-X. Hu, M.-L. Zhang, S.-M. Xin, W.-P. Jia, J. Zhao, G. Pei, β-arrestin-1 protein represses diet-induced obesity. *J. Biol. Chem.* **286**, 28396–28402 (2011).
20. J. Kim, C. A. Grotegut, J. W. Wisler, T. Li, L. Mao, M. Chen, W. Chen, P. B. Rosenberg, H. A. Rockman, R. J. Lefkowitz, β-arrestin 1 regulates β2-adrenergic receptor-mediated skeletal muscle hypertrophy and contractility. *Skelet. Muscle* **8**, 39 (2018).
21. J. Eguchi, X. Wang, S. Yu, E. E. Kershaw, P. C. Chiu, J. Dushay, J. L. Estall, U. Klein, E. Maratos-Flier, E. D. Rosen, Transcriptional control of adipose lipid handling by IRF4. *Cell Metab.* **13**, 249–259 (2011).
22. X. Kong, T. Yao, P. Zhou, L. Kazak, D. Tenen, A. Lyubetskaya, B. A. Dawes, L. Tsai, B. B. Kahn, B. M. Spiegelman, T. Liu, E. D. Rosen, Brown adipose tissue controls skeletal muscle function via the secretion of myostatin. *Cell Metab.* **28**, 631–643.e3 (2018).
23. S. M. Steculorum, J. Ruud, I. Karakasilioti, H. Backes, L. Engström Ruud, K. Timper, M. E. Hess, E. Tsaousidou, J. Mauer, M. C. Vogt, L. Paeger, S. Bremser, A. C. Klein, D. A. Morgan, P. Frommolt, P. T. Brinkkötter, P. Hammerschmidt, T. Benzing, K. Rahmouni, F. T. Wunderlich, P. Kloppenburg, J. C. Brüning, AgRP neurons control systemic insulin sensitivity via myostatin expression in brown adipose tissue. *Cell* **165**, 125–138 (2016).
24. D. L. Allen, D. S. Hittel, A. C. McPherron, Expression and function of myostatin in obesity, diabetes, and exercise adaptation. *Med. Sci. Sports Exerc.* **43**, 1828–1835 (2011).
25. B. B. Lowell, V. S-Susulic, A. Hamann, J. A. Lawitts, J. Himms-Hagen, B. B. Boyer, L. P. Kozak, J. S. Flier, Development of obesity in transgenic mice after genetic ablation of brown adipose tissue. *Nature* **366**, 740–742 (1993).
26. H. Sell, J. P. Berger, P. Samson, G. Castriota, J. Lalonde, Y. Deshaies, D. Richard, Peroxisome proliferator-activated receptor γ agonism increases the capacity for sympathetically mediated thermogenesis in lean and *ob/ob* mice. *Endocrinology* **145**, 3925–3934 (2004).
27. Y.-K. Park, L. Wang, A. Giampietro, B. Lai, J.-E. Lee, K. Ge, Distinct roles of transcription factors klf4, krox20, and peroxisome proliferator-activated receptor γ in adipogenesis. *Mol. Cell. Biol.* **37**, e00554–e00516 (2017).
28. W. Mo, L. Zhang, G. Yang, J. Zhai, Z. Hu, Y. Chen, X. Chen, L. Hui, R. Huang, G. Hu, Nuclear β-arrestin1 functions as a scaffold for the dephosphorylation of STAT1 and moderates the antiviral activity of IFN-γ. *Mol. Cell* **31**, 695–707 (2008).
29. C. Z. Hoeppner, N. Cheng, R. D. Ye, Identification of a nuclear localization sequence in β-arrestin-1 and its functional implications. *J. Biol. Chem.* **287**, 8932–8943 (2012).
30. D. Farré, R. Roset, M. Huerta, J. E. Adsuara, L. Roselló, M. M. Albà, X. Messeguer, Identification of patterns in biological sequences at the ALGGEN server: PROMO and MALGEN. *Nucleic Acids Res.* **31**, 3651–3653 (2003).
31. B. Luan, J. Zhao, H. Wu, B. Duan, G. Shu, X. Wang, D. Li, W. Jia, J. Kang, G. Pei, Deficiency of a β-arrestin-2 signal complex contributes to insulin resistance. *Nature* **457**, 1146–1149 (2009).
32. L. Zhu, J. Almaça, P. K. Dadi, H. Hong, W. Sakamoto, M. Rossi, R. J. Lee, N. C. Vierra, H. Lu, Y. Cui, S. M. McMillin, N. A. Perry, V. V. Gurevich, A. Lee, B. Kuo, R. D. Leapman, F. M. Matschinsky, N. M. Doliba, N. M. Urs, M. G. Caron, D. A. Jacobson, A. Caicedo, J. Wess, β-arrestin-2 is an essential regulator of pancreatic β-cell function under physiological and pathophysiological conditions. *Nat. Commun.* **8**, 14295 (2017).
33. L. Zhu, M. Rossi, Y. Cui, R. J. Lee, W. Sakamoto, N. A. Perry, N. M. Urs, M. G. Caron, V. V. Gurevich, G. Godlewski, G. Kunos, M. Chen, W. Chen, J. Wess, Hepatic β-arrestin 2 is essential for maintaining euglycemia. *J. Clin. Invest.* **127**, 2941–2945 (2017).
34. P. Seale, B. Bjork, W. Yang, S. Kajimura, S. Chin, S. Kuang, A. Scimè, S. Devarakonda, H. M. Conroe, H. Erdjument-Bromage, P. Tempst, M. A. Rudnicki, D. R. Beier, B. M. Spiegelman, PRDM16 controls a brown fat/skeletal muscle switch. *Nature* **454**, 961–967 (2008).
35. S. Kajimura, P. Seale, K. Kubota, E. Lunsford, J. V. Frangioni, S. P. Gygi, B. M. Spiegelman, Initiation of myoblast to brown fat switch by a PRDM16-C/EBP-β transcriptional complex. *Nature* **460**, 1154–1158 (2009).

36. J. A. Timmons, K. Wennmalm, O. Larsson, T. B. Walden, T. Lassmann, N. Petrovic, D. L. Hamilton, R. E. Gimeno, C. Wahlestedt, K. Baar, J. Nedergaard, B. Cannon, Myogenic gene expression signature establishes that brown and white adipocytes originate from distinct cell lineages. *Proc. Natl. Acad. Sci. U.S.A.* **104**, 4401–4406 (2007).
37. S. J. Lee, A. C. McPherron, Myostatin and the control of skeletal muscle mass. *Curr. Opin. Genet. Dev.* **9**, 604–607 (1999).
38. A. C. McPherron, A. M. Lawler, S. J. Lee, Regulation of skeletal muscle mass in mice by a new TGF-beta superfamily member. *Nature* **387**, 83–90 (1997).
39. B. Fournier, B. Murray, S. Gutzwiller, S. Marcaletti, D. Marcellin, S. Bergling, S. Brachat, E. Persohn, E. Pierrel, F. Bombard, S. Hatakeyama, A.-U. Trendelenburg, F. Morvan, B. Richardson, D. J. Glass, E. Lach-Trifilieff, J. N. Feige, Blockade of the activin receptor IIb activates functional brown adipogenesis and thermogenesis by inducing mitochondrial oxidative metabolism. *Mol. Cell. Biol.* **32**, 2871–2879 (2012).
40. M. Braga, S. Pervin, K. Norris, S. Bhasin, R. Singh, Inhibition of in vitro and in vivo brown fat differentiation program by myostatin. *Obesity (Silver Spring)* **21**, 1180–1188 (2013).
41. M. Ji, Q. Zhang, J. Ye, X. Wang, W. Yang, D. Zhu, Myostatin induces p300 degradation to silence *cyclin D1* expression through the PI3K/PTEN/Akt pathway. *Cell. Signal.* **20**, 1452–1458 (2008).
42. L.-N. Zhuang, W.-X. Hu, S.-M. Xin, J. Zhao, G. Pei, β-arrestin-1 protein represses adipogenesis and inflammatory responses through its interaction with peroxisome proliferator-activated receptor-γ (PPARγ). *J. Biol. Chem.* **286**, 28403–28413 (2011).
43. C. Wang, X. Zeng, Z. Zhou, J. Zhao, G. Pei, β-arrestin-1 contributes to brown fat function and directly interacts with PPARα and PPARγ. *Sci. Rep.* **6**, 26999 (2016).
44. J. Lin, H. B. Arnold, M. A. Della-Fera, M. J. Azain, D. L. Hartzell, C. A. Baile, Myostatin knockout in mice increases myogenesis and decreases adipogenesis. *Biochem. Biophys. Res. Commun.* **291**, 701–706 (2002).
45. C. Zhang, C. McFarlane, S. Lokireddy, S. Masuda, X. Ge, P. D. Gluckman, M. Sharma, R. Kambadur, Inhibition of myostatin protects against diet-induced obesity by enhancing fatty acid oxidation and promoting a brown adipose phenotype in mice. *Diabetologia* **55**, 183–193 (2012).
46. J. Dong, Y. Dong, Y. Dong, F. Chen, W. E. Mitch, L. Zhang, Inhibition of myostatin in mice improves insulin sensitivity via irisin-mediated cross talk between muscle and adipose tissues. *Int. J. Obes.* **40**, 434–442 (2016).
47. B. Deng, F. Zhang, J. Wen, S. Ye, L. Wang, Y. Yang, P. Gong, S. Jiang, The function of myostatin in the regulation of fat mass in mammals. *Nutr. Metab. (Lond)* **14**, 29 (2017).
48. S. Reisz-Porszasz, S. Bhasin, J. N. Artaza, R. Shen, I. Sinha-Hikim, A. Hogue, T. J. Fielder, N. F. Gonzalez-Cadavid, Lower skeletal muscle mass in male transgenic mice with muscle-specific overexpression of myostatin. *Am. J. Physiol. Endocrinol. Metab.* **285**, E876–E888 (2003).
49. S. Jain, I. Ruiz de Azua, H. Lu, M. F. White, J.-M. Guettier, J. Wess, Chronic activation of a designer G_q-coupled receptor improves β cell function. *J. Clin. Invest.* **123**, 1750–1762 (2013).
50. S. M. Steculorum, K. Timper, L. Engström Ruud, N. Evers, L. Paeger, S. Bremser, P. Kloppenburg, J. C. Brüning, Inhibition of P2Y6 signaling in AgRP neurons reduces food intake and improves systemic insulin sensitivity in obesity. *Cell Rep.* **18**, 1587–1597 (2017).
51. J. K. Kim, O. Gavrilova, Y. Chen, M. L. Reitman, G. I. Shulman, Mechanism of insulin resistance in A-ZIP/F-1 fatless mice. *J. Biol. Chem.* **275**, 8456–8460 (2000).
52. M. Rossi, L. Zhu, S. M. McMillin, S. P. Pydi, S. Jain, L. Wang, Y. Cui, R. J. Lee, A. H. Cohen, H. Kaneto, M. J. Birnbaum, Y. Ma, Y. Rotman, J. Liu, T. J. Cyphert, T. Finkel, O. P. McGuinness, J. Wess, Hepatic G_i signaling regulates whole-body glucose homeostasis. *J. Clin. Invest.* **128**, 746–759 (2018).
53. J. J. Wilkes, D. J. Lloyd, N. Gekakis, Loss-of-function mutation in myostatin reduces tumor necrosis factor alpha production and protects liver against obesity-induced insulin resistance. *Diabetes* **58**, 1133–1143 (2009).
54. J. H. Youn, J. K. Kim, T. A. Buchanan, Time courses of changes in hepatic and skeletal muscle insulin action and GLUT4 protein in skeletal muscle after STZ injection. *Diabetes* **43**, 564–571 (1994).
55. J. E. Ayala, D. P. Bracy, O. P. McGuinness, D. H. Wasserman, Considerations in the design of hyperinsulinemic-euglycemic clamps in the conscious mouse. *Diabetes* **55**, 390–397 (2006).

Acknowledgments

Funding: This research was funded by the Intramural Research Program of the National Institute of Diabetes and Digestive and Kidney Diseases (NIDDK, NIH). We thank Y. Ma and N. Liu (Mouse Metabolism Core, NIDDK) for technical assistance with some of the metabolic studies, H. Smith, I. Akan, and S. Yun (NIDDK Genomics Core) for help with the RNA-seq work, G. Godlewski in G. Kunos' laboratory (NIAAA, NIH) for assistance with the hyperinsulinemic-euglycemic clamp studies, and K. Ge for providing the immortalized mouse brown pre-adipocyte ceil line. J. Reece (NIDDK Advanced Light Microscopy & Image Analysis Core) provided helpful advice regarding the imaging studies. The Mstn-AB was a gift from R. S. Pearsall (Acceleron Pharma, Cambridge, MA). R. Lefkowitz (Duke University, Durham, NC) provided us with the *barr1 f/f* mice. **Author contributions:** S.P.P. and J.W. designed the study, researched data, and wrote the manuscript. S.P.P., S.J., L.F.B., L.Z., W.S., J.M., L.W., Y.C., H.L., and O.G. carried out experiments and interpreted and analyzed experimental data. **Competing interests:** The authors declare that they have no competing interests. **Data and materials availability:** All data needed to evaluate the conclusions in the paper are present in the paper and/or the Supplementary Materials. Additional data related to this paper may be requested from the authors.

Submitted 11 November 2019
Accepted 16 April 2020
Published 5 June 2020
10.1126/sciadv.aba1733

Citation: S. P. Pydi, S. Jain, L. F. Barella, L. Zhu, W. Sakamoto, J. Meister, L. Wang, H. Lu, Y. Cui, O. Gavrilova, J. Wess, β-arrestin-1 suppresses myogenic reprogramming of brown fat to maintain euglycemia. *Sci. Adv.* **6**, eaba1733 (2020).